Original Article

Spectral CT imaging as a new quantitative tool? Assessment of perfusion defects of pulmonary parenchyma in patients with lung cancer

Ying-Shi Sun, Xiao-Yan Zhang, Yong Cui, Lei Tang, Xiao-Ting Li, Ying Chen, Xiao-Peng Zhang

Key Laboratory of Carcinogenesis and Translational Research (Ministry of Education), Department of Radiology, Peking University Cancer Hospital & Institute, Beijing 100142, China

Corresponding to: Xiao-Peng Zhang. Key Laboratory of Carcinogenesis and Translational Research (Ministry of Education), Department of Radiology, Peking University Cancer Hospital & Institute, No.52 Fucheng Road, Haidian District, Beijing 100142, China. Email: zxp@bjcancer.org.

Objective: This study investigated the capability of dual-energy spectral computed tomography (CT) to quantitatively evaluate lung perfusion defects that are induced by central lung cancer.

Methods: Thirty-two patients with central lung cancer underwent CT angiography using spectral imaging. A univariate general linear model was conducted to analyze the variance of iodine concentration/CT value with three factors of lung fields. A paired *t*-test was used to compare iodine concentrations and CT values between the distal end of lung cancer and the corresponding area in the contralateral normal lung.

Results: Iodine concentrations increased progressively in the far, intermediate and near ground sides in the normal lung fields at 0.60±0.28, 0.93±0.27 and 1.25±0.38 mg/mL, respectively (P<0.001). The same trend was observed for the CT values [–(840.64±49.08), –(812.66±50.85) and –(760.83±89.17) HU, P<0.001]. The iodine concentration (0.70±0.42 mg/mL) of the lung field in the distal end of lung cancer was significantly lower than the corresponding area in the contralateral normal lung (1.19±0.62 mg/mL) (t=–7.23, P<0.001). However, the CT value of lung field in the distal end of lung cancer was significantly higher than the corresponding area in the contralateral normal lung [–(765.29±93.34) HU *vs.* –(800.07±76.18) HU, t=3.564, P=0.001].

Conclusions: Spectral CT imaging based on the spectral differentiation of iodine is feasible and can quantitatively evaluate pulmonary perfusion and identify perfusion defects that are induced by central lung cancer. Spectral CT seems to be a promising technique for the simultaneous evaluation of both morphological and functional lung information.

Keywords: Spectral; computed tomography (CT); quantitative analysis; perfusion; lung cancer

Submitted Aug 17, 2013. Accepted for publication Oct 28, 2013.
doi: 10.3978/j.issn.1000-9604.2013.12.01
Scan to your mobile device or view this article at: http://www.thecjcr.org/article/view/3077/3979

Introduction

There is a very close relationship between pulmonary ventilation and perfusion. Most pathological conditions of the pulmonary parenchyma alter blood flow in the pulmonary capillary system or the aeration of the alveolar system.

Computed tomography (CT) is the first-line imaging modality for the evaluation of thoracic disorders. Significant technical progress has been made in efficiently capturing morphological and functional lung information. There has been no routinely used imaging modality that enables the imaging of aeration and blood perfusion in one examination until dual-energy CT (DECT) emergence.

For functional imaging, DECT using dual-source CT (DSCT) systems with two independent tube-detector units improves the feasibility of material differentiation (1-3). Much research has been conducted on DECT for pulmonary thromboembolism diagnosis (4-11). Chae's study indicated a good correlation between the right/left ventricle diameter ratio and the perfusion defect score (7). Another study by Krissak *et al.* suggested a superior diagnostic value of perfusion images obtained by DECT (8). Several recent

Table 1 Patients' characteristics and histopathological evaluation

Characteristics and histopathological evaluation	Value
Number of patients	32
Mean age [range] (year)	58.6 [36-86]
Female	63.1 [37-86]
Male	57.0 [36-73]
Female:male	8:24
Histopathological diagnosis	
Squamous cell carcinoma	17
Adenocarcinoma	10
Small cell lung cancer	5
Location of lesion	
Superior lobe of right lung	10
Middle lobe of right lung	0
Inferior lobe of right lung	6
Superior and middle lobe of right lung	1
Middle and inferior lobe of right lung	1
Superior and inferior lobe of right lung	0
Superior, middle and inferior lobe of right lung	2
Superior lobe of left lung	8
Inferior lobe of left lung	2
Superior and inferior lobe of left lung	2

studies using Xenon DECT have provided evidence for the use of ventilation-perfusion CT images or parameters (12-16).

DECT encounters barriers to widespread clinical use because of motion misregistration, high image noise, and excessive radiation exposure from longer acquisition times (17). Spectral CT may be a solution to this problem. The CT scanner applies a rapid kilovoltage switching technique with single source X-ray. This scanning mode enables the precise registration of data sets for the creation of accurate material-decomposition images (e.g., water- and iodine-based material decomposition images) and monochromatic spectral images at energy levels ranging from 40 to 140 kV. The use of the material decomposition technique with spectral CT showed that the iodine concentration could be obtained quantitatively from the iodine-attenuation images, which probably reflected lung perfusion.

Central lung cancer often involves lobar bronchi, segmental bronchi, and distal lung ventilation disorder, which leads to slight atelectasis, and complete atelectasis in severe cases. Ventilation and perfusion defects of the corresponding distal lung tissue may also be present. Spectral CT not only provides morphologic images, but also serves as an effective tool for the quantitative evaluation of lung perfusion and ventilation defects.

The purpose of this preliminary study was to investigate the capability of spectral CT to quantitatively evaluate lung perfusion defects that are induced by central lung cancers.

Materials and methods

Patients

This prospective study was approved by the institutional review board of Beijing Cancer Hospital, and written informed consent was obtained from all patients.

From January 2011 to August 2011, 79 patients known or suspected primary lung carcinoma underwent multiple-phase CT scanning in a GE Discovery CT750 HD CT scanner (GE Medical Systems, Milwaukee, WI, USA). Inclusion criteria were a primary central lung cancer as demonstrated by biopsy with a bronchoscope. The exclusion criteria included: (I) previous surgery or chemoradiotherapy (n=3); (II) combined with atelectasis (n=32); and (III) associated with other lung diseases (n=12). Thus, a total of 32 consecutive patients who met the study criteria were recruited from our clinics. Patients' characteristics and histopathological evaluations are summarized in *Table 1*.

CT protocol

All patients underwent scanning with spectral CT imaging by standard protocol. CT was performed during a breath hold following deep inspiration with the patient in the supine position. Before scanning, each patient was carefully instructed on how to breathe during scanning.

Each patient underwent a one-phase contrast-enhanced CT examination. Patients were administrated non-ionic contrast material with antecubital venous access at a rate of 3-4 mL/s (1.5 mL/kg, iohexol 300 mg I/mL, Omnipaque, GE Healthcare). A total of 90-120 mL contrast material was injected during the pulmonary arterial phase. The scanning delay for the pulmonary artery phase imaging was determined using automated scan-triggering software. Pulmonary arterial phase scanning began 5 s after the trigger attenuation threshold (100 HU) was reached at the level of the pulmonary artery.

Pulmonary artery phase scanning was performed in the spectral imaging mode. Other parameters comprised:

Table 2 Actual and measured iodine concentrations in *in vitro* experiments

	Actual iodine concentrations (mg/mL)	Measured iodine concentrations (mg/mL)
1	30	30.51
2	20	20.02
3	10	9.96
4	5	5.12
5	2	1.96
6	1	1.08
7	0.5	0.42

collimation thickness 5 mm, reconstructed thickness 0.625 mm, tube current 640 mA, rotation speed 0.6 s, helical pitch 1.375, and CT dose index volume 17.65 mGy.

The CT images were reconstructed using material decomposition software. The adaptive statistical iterative reconstruction algorithm was applied to suppress image noise in the decomposition images. Three types of images were reconstructed from the single spectral CT acquisition, water- and iodine-based material decomposition images, and monochromatic images obtained at different energy levels, ranging from 40 to 140 kV.

CT image quantitative analysis

An *in vitro* experiment was performed to evaluate the accuracy of iodine concentration measurements obtained with the spectral images. A set of seven test tubes containing different known iodine concentrations, from 0.5 to 30.0 mg/mL, were scanned by spectral imaging protocol. The iodine concentrations were measured using a circular region of interest (ROI) in the test tube cross section on the iodine-based material decomposition images. The spectral imaging-measured iodine concentrations were compared with the true concentrations in the test tubes. A radiologist (with five years experience in clinical CT) performed the quantitative measurements using a spectral imaging viewer (GSI Viewer; GE Healthcare) to analyze the material decomposition images.

CT images were analyzed by the consensus of two experienced radiologists (with 15 years and 5 years experience in clinical CT, respectively) who worked together on a workstation (AW4.4; GE Medical Systems, Milwaukee, WI, USA) and were blinded to the clinical information of patients. The quantitative analysis of iodine concentration was analyzed using the spectral imaging viewer software.

For each patient, a ROI (number of pixels ≥100) was placed in the lung parenchyma in the distal end of central lung cancer and the contralateral corresponding lung region, the pulmonary parenchyma of the level of the apex, the hilum, and the superior phrenic of the lungs on both sides (far, intermediate, and near ground sides of normal lung fields). The iodine concentrations and the CT value of the corresponding pulmonary parenchyma were derived from the iodine-based material decomposition images and the lung window images, respectively.

To ensure consistency, all measurements were performed three times at different image levels, and the average values were calculated. For all measurements, the size, shape, and position of the ROI were consistent between the lung window images and the iodine-based material decomposition images as confirmed using the copy-and-paste function.

Statistical analysis

All statistical analyses were performed using the SPSS software (SPSS for Windows, Ver.11.5; SPSS Inc., Chicago, IL, USA). Data were expressed as $\bar{x}\pm s$.

A univariate general linear model (GLM) was conducted to analyze the variance of iodine concentration/CT value with the three factors from lung fields. The three factors, which served as fixed factors, were the apex-hilar-superior phrenic of lungs, the far, intermediate, and near ground sides of the vertical location and the right-left lungs. The effects of these factors on iodine concentration/CT value were tested. The least significant difference (LSD) test evaluated differences between specific means when the overall F test showed significance. The paired *t*-test was used to compare the means of iodine concentrations and CT values between the distal end of lung cancer and the corresponding area in the contralateral normal lung.

Two-tailed P values were used, and statistical significance was confirmed if the P value was less than an alpha (α) level of 0.05.

Results

We observed excellent agreement between the measured and actual iodine concentrations in the *in vitro* experiments (*Table 2*).

The iodine concentration of lung parenchyma in the

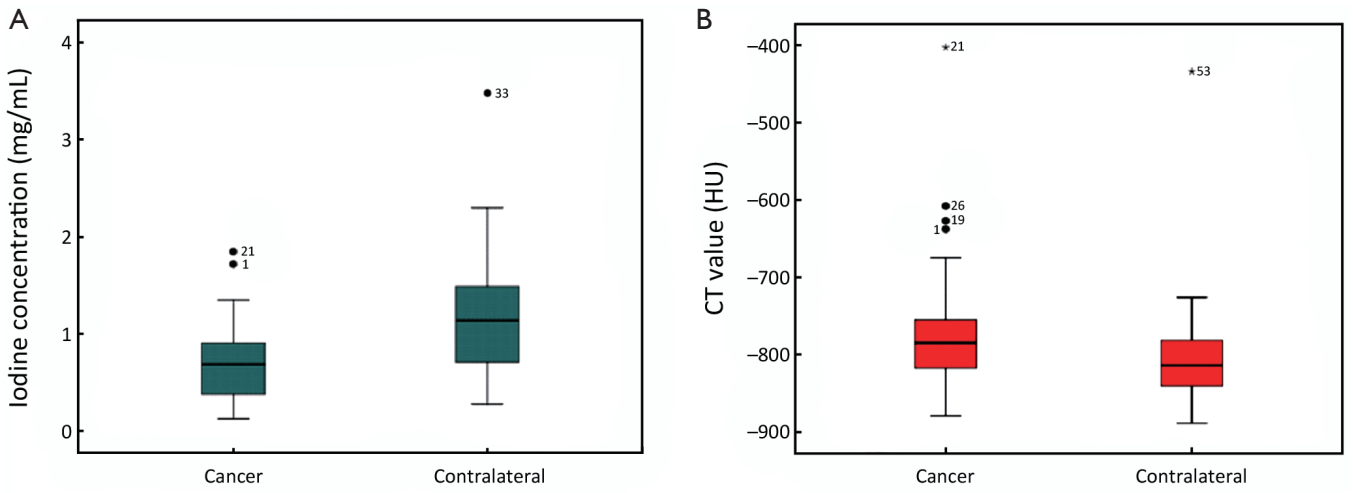

Figure 1 Box plot demonstrates iodine concentrations and computed tomography (CT) values of lung tissue at the distal end of the cancer and in the contralateral healthy lung field. Cancer, iodine concentrations/CT values of lung tissue at the distal end of the cancer; contralateral, iodine concentrations/CT values of corresponding lung tissue in contralateral healthy lung field. The cancer iodine concentration was significantly lower than the contralateral (A); the cancer CT value was significantly higher than the contralateral (B).

distal end of central lung cancer was significantly lower than the corresponding area in the contralateral healthy lung parenchyma (0.70±0.42 mg/mL *vs.* 1.19±0.62 mg/mL, t=–7.231, P<0.001). However, the CT value of lung parenchyma in the distal end of lung cancer was statistically higher than the corresponding area in the contralateral healthy lung parenchyma [–(765.29±93.34) HU *vs.* –(800.07±76.18) HU, t=3.564, P=0.001). (*Figures 1,2*)

The iodine concentrations and CT values of normal lung fields are shown in *Table 3* and demonstrated the far, intermediate and near ground sides in the apex, hilar and superior phrenic of lung tissue, respectively.

A univariate GLM was conducted to analyze the variance of iodine concentration with the three factors from lung fields, which were apex-hilar-superior phrenic of lung, far-intermediate-near ground side of vertical location and right-left lung. The results demonstrated that iodine concentrations varied among the far, intermediate, and near ground sides of normal lung fields (F=156.393, P<0.001). The LSD test showed a significant difference of iodine concentrations in comparison between any two groups, and iodine concentrations increased progressively in the far, intermediate and near ground sides of normal lung fields at 0.60±0.28, 0.93±0.27 and 1.25±0.38 mg/mL, respectively (P<0.001).

The result of univariate GLM also showed that CT values varied among far, intermediate and near ground sides of normal lung fields (F=57.915, P<0.001) with a significant difference between any two groups (P<0.001). The same trend as iodine concentrations was observed in CT values in the far, intermediate and near ground sides of normal lung fields [–(840.64±49.08), –(812.66±50.85) and –(760.83±89.17) HU, respectively].

Discussion

In the diagnostic energy range, there are two dominant ways that X-ray photons interact with matter: the photoelectric effect and Compton scatter. In the low-energy range, the X-ray interaction is predominately photoelectric, but in the high-energy range, the Compton scatter is dominant. By taking measurements at both polychromatic energy levels, we obtained an object's photoelectric and Compton characteristics from which we could uniquely identify and differentiate the material. This is in contrast to conventional CT in which a single measurement is taken with X-ray photons generated by a particular X-ray tube voltage (kVp) setting. This measurement permits the calculation of only a single parameter to represent a material, namely its density. Two different material compounds can have identical densities, and it is impossible for conventional CT to differentiate between such materials. However, using dual-energy or spectral CT, two projection measurements are acquired. Unique materials can be better characterised, and two different materials can be distinguished more uniquely

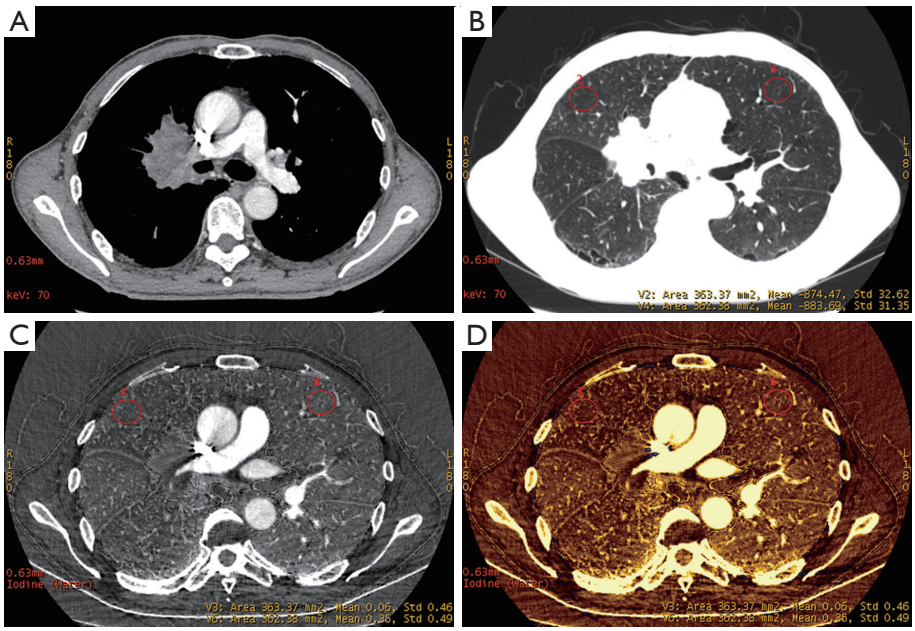

Figure 2 Computed tomography (CT) images of a 72-year-old male with primary central lung squamous cell carcinoma. (A) Axial image (mediastinal window) showed a right central bronchogenic carcinoma with heterogeneous enhancement; (B) Lung window; (C,D) Iodine images acquired using gemstone spectral imaging. The CT value of right upper lung parenchyma (–874 HU) in the distal end of lung cancer was higher than the corresponding area in the contralateral healthy lung parenchyma (–884 HU), which was measured in the lung window image. There was no perceptive difference between those two areas on the iodine image, but the iodine concentration of right upper lung parenchyma (0.06 mg/mL) in the distal end of lung cancer was significantly lower than that of the corresponding area in the contralateral healthy lung parenchyma (0.35 mg/mL), which represented the perfusion defect caused by right central bronchogenic carcinoma.

Table 3 Iodine concentrations and CT values of normal lung fields

		Iodine concentrations (mg/mL)		CT (HU)	
		Right lung	Left lung	Right lung	Left lung
Apex	Far	0.71±0.24	0.71±0.22	–(836.73±30.49)	–(834.59±26.57)
	Intermediate	0.95±0.30	0.88±0.22	–(828.20±30.48)	–(825.98±39.65)
	Near	1.34±0.45	1.17±0.30	–(784.26±39.12)	–(787.03±59.97)
Hilar	Far	0.59±0.25	0.60±0.28	–(841.31±33.18)	–(837.51±41.63)
	Intermediate	0.91±0.29	0.86±0.27	–(817.24±54.94)	–(816.33±37.13)
	Near	1.26±0.46	1.29±0.36	–(745.47±100.57)	–(756.44±102.36)
Superior phrenic	Far	0.45±0.27	0.57±0.33	–(864.42±30.29)	–(830.22 ±87.75)
	Intermediate	0.97±0.28	1.01±0.28	–(809.45±46.00)	–(787.53±72.40)
	Near	1.23±0.38	1.21±0.36	–(744.40±96.00)	–(757.94±98.81)

and reliably (18,19).

Given the span of atomic numbers, water and iodine are commonly selected as the basis pair when using the material decomposition technique to represent common materials within the range of atomic numbers, and soft tissue and iodinated contrast material are used to create material attenuation images. In our phantom study, the result showed excellent agreement between the measured and actual iodine concentrations, thus suggesting that the relative spectral parameters computed *in vivo* cannot

be attributed to a systematic error based on our scanning design, and it might be a useful parameter.

For normal lung tissue, the CT scan is conducted in the supine position, and the blood flow of the near-side lung is relatively greater than the distant side due to gravity; however, the gas content should be relatively lower. If the iodine concentration reflects lung perfusion and the CT value reflects the gas content of lung tissue, the CT value and the iodine value should show a gradual increase in normal lung tissue from the remote side to the near side in the supine position. In our study, the results showed that the distribution of iodine concentration in normal lung tissue had no relationship with the upper, middle, or lower lung or the left and right lung, but was only correlated with the far and near ground sides. Iodine concentrations in the far, intermediate and near ground sides were 0.60±0.28, 0.93±0.27, 1.25±0.38 mg/mL, respectively, which shows a gradually increasing trend that is similar to the changes in CT values. Therefore, the application of the iodine concentration, the CT value and relevant changes can reflect the state of pulmonary perfusion and ventilation.

Our results suggested that the CT value of lung parenchyma in the distal end of lung cancer was statistically higher than the corresponding area of the contralateral healthy lung parenchyma, mainly because of distal lung ventilation defects that is induced by central lung cancer involving lobar or segmental bronchi. We also found that the iodine concentration of lung parenchyma in the distal end of central lung cancer was significantly lower than the corresponding area of the contralateral healthy lung parenchyma, which suggested an obvious perfusion defect in the distal end of lung cancer. The ventilation/perfusion defect was usually revealed in the distal end of lung cancer, which was generally explained as follows: (I) direct pressure to the pulmonary artery led to arterial lumen stenosis or the complete occlusion of the lumen in severe cases; (II) vascular intimal hyperplasia or fibrosis that was stimulated by the nearby tumour occurred in the artery; and (III) bronchial tumor compression resulted in inadequate ventilation and the corresponding distal lung tissue hypoxia, which led to a compensatory reduction in arterial perfusion.

Our study indicated a higher CT value with lower iodine concentrations at the distal end of central lung cancer as a result of the remote ventilation defects. The differences in the CT value and iodine concentrations suggested that the two parameters reflect different characteristics of tissues. The CT value represents the attenuation of tissues, and the greater the condensing of the tissues, the higher its CT values. Therefore, higher CT values at the distal end of central lung cancer indicate that the lung tissues are becoming more condensed as a consequence of ventilation defects. The iodine concentration in spectral CT imaging was derived using the iodine-based material decomposition formula but not through the direct measurement of true iodine. In previous studies, Lv *et al*. concluded that the iodine concentration in lesions acquired in this manner is a quantitative parameter that is highly precise, and they indicated that it would probably act as an effective indicator for blood perfusion (20). Therefore, we believed that the iodine concentration would indirectly reflect real blood perfusion rather than the tissue density. Based on this belief, we presumed that the lower iodine concentration indicated a decrease in local blood perfusion. Therefore, spectral CT allows the application of one CT screening equipment to complete the simultaneous evaluation of lung morphology and functional information, such as lung ventilation and perfusion.

Our study still had several limitations. One major limitation was the absence of nuclear medicine lung perfusion imaging as standard of reference that limited our ability to evaluate diagnostic accuracy. A further limitation was the rather small study population with variable indications. In addition, we could not include healthy volunteers with normal lung tissue as control due to the small number of patients without carcinoma in our hospital that required an enhanced chest CT.

In conclusion, our results indicate that spectral CT imaging based on the spectral differentiation of iodine is technically feasible and can quantitatively evaluate pulmonary perfusion and identify perfusion defects induced by central lung cancer. Spectral CT seems to be a promising, non-invasive technique for the evaluation of lung morphology and functional information simultaneously, such as lung ventilation and perfusion.

Acknowledgements

This work was supported by National Natural Science Foundation of China (Grant No. 81071129, 30970825) and the National Basic Research Program of China (973 Program) (Grant No. 2011CB707705).
Disclosure: The authors declare no conflict of interest.

References

1. Fuchs TA, Sah BR, Stehli J, et al. Attenuation correction

maps for SPECT myocardial perfusion imaging from contrast-enhanced coronary CT angiography: gemstone spectral imaging with single-source dual energy and material decomposition. J Nucl Med 2013;54:2077-80.
2. Mileto A, Marin D, Nelson RC, et al. Dual energy MDCT assessment of renal lesions: an overview. Eur Radiol 2013. [Epub ahead of print].
3. Srinivasan A, Hoeffner E, Ibrahim M, et al. Utility of dual-energy CT virtual keV monochromatic series for the assessment of spinal transpedicular hardware-bone interface. AJR Am J Roentgenol 2013;201:878-83.
4. Gorgos A, Remy-Jardin M, Duhamel A, et al. Evaluation of peripheral pulmonary arteries at 80 kV and at 140 kV: dual-energy computed tomography assessment in 51 patients. J Comput Assist Tomogr 2009;33:981-86.
5. Lee CW, Seo JB, Song JW, et al. Evaluation of computer-aided detection and dual energy software in detection of peripheral pulmonary embolism on dual-energy pulmonary CT angiography. Eur Radiol 2011;21:54-62.
6. Lu GM, Wu SY, Yeh BM, et al. Dual-energy computed tomography in pulmonary embolism. Br J Radiol 2010;83:707-18.
7. Krissak R, Henzler T, Reichert M, et al. Enhanced visualization of lung vessels for diagnosis of pulmonary embolism using dual energy CT angiography. Invest Radiol 2010;45:341-6.
8. Chae EJ, Seo JB, Jang YM, et al. Dual-energy CT for assessment of the severity of acute pulmonary embolism: pulmonary perfusion defect score compared with CT angiographic obstruction score and right ventricular/left ventricular diameter ratio. AJR Am J Roentgenol 2010;194:604-10.
9. Fink C, Johnson TR, Michaely HJ, et al. Dual-energy CT angiography of the lung in patients with suspected pulmonary embolism: initial results. Rofo 2008;180:879-83.
10. Pontana F, Faivre JB, Remy-Jardin M, et al. Lung perfusion with dual-energy multidetector -row CT (MDCT): feasibility for the evaluation of acute pulmonary embolism in 117 consecutive patients. Acad Radiol 2008;15:1494-504.
11. Renard B, Remy-Jardin M, Santangelo T, et al. Dual-energy CT angiography of chronic thromboembolic disease: can it help recognize links between the severity of pulmonary arterial obstruction and perfusion defects? Eur J Radiol 2011;79:467-72.
12. Park EA, Goo JM, Park SJ, et al. Chronic obstructive pulmonary disease: quantitative and visual ventilation pattern analysis at xenon ventilation CT performed by using a dual-energy technique. Radiology 2010;256:985-97.
13. Thieme SF, Hoegl S, Nikolaou K, et al. Pulmonary ventilation and perfusion imaging with dual-energy CT. Eur Radiol 2010;20:2882-9.
14. Chae EJ, Seo JB, Lee J, et al. Xenon ventilation imaging using dual-energy computed tomography in asthmatics: initial experience. Invest Radiol 2010;45:354-61.
15. Chae EJ, Seo JB, Goo HW, et al. Xenon ventilation CT with a dual-energy technique of dual-source CT: initial experience. Radiology 2008;248:615-24.
16. Ferda J, Ferdová E, Mírka H, et al. Pulmonary imaging using dual-energy CT, a role of the assessment of iodine and air distribution. Eur J Radiol 2011;77:287-93.
17. Graser A, Johnson TR, Hecht EM, et al. Dual-energy CT in patients suspected of having renal masses: can virtual nonenhanced images replace true nonenhanced images? Radiology 2009;252:433-40.
18. Brooks RA. A quantitative theory of the Hounsfield unit and its application to dual energy scanning. J Comput Assist Tomogr 1977;1:487-93.
19. Hawkes DJ, Jackson DF, Parker RP. Tissue analysis by dual-energy computed tomography. Br J Radiol 1986;59:537-42.
20. Lv P, Lin XZ, Li J, et al. Differentiation of small hepatic hemangioma from small hepatocellular carcinoma: recently introduced spectral CT method. Radiology 2011;259:720-9.

Cite this article as: Sun YS, Zhang XY, Cui Y, Tang L, Li XT, Chen Y, Zhang XP. Spectral CT imaging as a new quantitative tool? Assessment of perfusion defects of pulmonary parenchyma in patients with lung cancer. Chin J Cancer Res 2013;25(6):722-728. doi: 10.3978/j.issn.1000-9604.2013.12.01

